Optical anisotropic-dielectric response of mercuric iodide

Huade Yao
Center for Microelectronic and Optical Materials Research and Department of Electrical Engineering, University of Nebraska, Lincoln, Nebraska 68588-0511

Blaine Johs
J. A. Woollam Company, Inc., Lincoln, Nebraska 68508

Ralph B. James
Sandia National Laboratories, Livermore, California 94551-0969

(Received 2 June 1997)

Anisotropic optical properties of mercuric iodide (HgI_2) were studied by variable-angle spectroscopic ellipsometry (VASE). Angular-dependent polarized reflectance and transmittance at three special optical-axis configurations, concerning the uniaxial anisotropic nature of the crystal, were derived to facilitate the VASE analysis. Two surface orientations of this tetragonal crystal were selected, i.e., an a-plane and a c-plane sample. Room-temperature multiple-angle spectroscopic ellipsometry measurements from both samples with three different optical configurations along with polarized transmission measurements were jointly analyzed by the VASE analysis through multiple-sample, multiple-model methods. Anisotropic dielectric functions of single-crystal HgI_2, $\varepsilon_{\perp}(\omega)$ and $\varepsilon_{\parallel}(\omega)$, for optical electric-field vector oriented perpendicular and parallel to the c axis, respectively, were obtained in the range 1.24–5.1 eV. Different absorption energy-band edges, at room temperature, were observed from the ordinary and extraordinary dielectric responses at 2.25 and 2.43 eV, respectively. This is consistent with the results related to the optical transitions between the conduction band and the heavy- and light-hole valence band indicated by theoretical studies. A surface model related to the surface roughness and defects of HgI_2 was established and characterized by the VASE analysis. [S0163-1829(97)05539-2]

I. INTRODUCTION

Crystal mercuric iodide (HgI_2) is an important technological material for room-temperature radiation (i.e., gamma and x ray) detectors.[1–5] It also presents some interesting scientific issues regarding its tetragonal crystal structures. The optical anisotropic behavior was observed via the reflectance and absorption spectra of HgI_2 crystal when the optical electric-field vectors **E** oriented parallel and perpendicular to the c axis.[6–11] The imaginary part of the dielectric functions $\varepsilon_{2\perp}(\omega)$ ($\mathbf{E}\perp c$) were deduced from the reflectivity spectra by means of Kramers-Kronig (KK) relations under several assumptions.[10] However, the optical anisotropic dielectric response of this crystal, such as dielectric functions ($\varepsilon=\varepsilon_1+\varepsilon_2$), have not been determined directly by precise optical measurements. Since HgI_2 crystal is tetragonal, it must be described by two dielectric-response functions, $\varepsilon_{\perp}(\omega)$ and $\varepsilon_{\parallel}(\omega)$, for optical electric-field vector oriented perpendicular (ordinary) and parallel (extraordinary) to the c axis, respectively. One frequently encountered difficulty is to calculate and analyze the optical measurement results in dealing with the uniaxial anisotropic nature of the crystal.

In this paper, we report the determination of room-temperature anisotropic dielectric functions $\varepsilon_{\perp}(\omega)$ and $\varepsilon_{\parallel}(\omega)$ of HgI_2 crystal in the range 1.24–5.1 eV, by variable-angle spectroscopic ellipsometry (VASE). The optical functions were extracted from simultaneous analysis of VASE measurements of two HgI_2 crystal samples: one c-plane surface, to which the c axis of the crystal is perpendicular; and another a-plane surface, to which the c axis is parallel. An analytical angular-dependent polarized reflectance and transmittance at three special optical-axis configurations, for the uniaxial anisotropic crystal were derived and a surface model concerning the roughness and possible near-surface defects was established for the VASE analyses. Room-temperature energy-band absorption edges of the HgI_2 crystal from the ordinary and extraordinary dielectric response will be discussed and presented.

II. EXPERIMENTAL DETAILS

A. Sample preparations

Two HgI_2 surfaces from this tetragonal crystal were prepared for the VASE measurements: a c-plane surface, to which the c axis of the crystal is perpendicular, and an a-plane surface, to which the c axis is parallel. Three special optical configurations were chosen for the VASE measurements: a c-plane surface, i.e., the c axis is normal to the sample surface, which we term here as c-p configuration; an a-plane surface with c axis is in the plane of sample surface and parallel to the plane of incidence, aEp configuration; and an a-plane surface with the c axis perpendicular to the plane of incidence, aEs configuration.

Sliced and polished c-plane and a-plane HgI_2 samples were subjected to a chemical etching to ensure clean and fresh surface before the VASE measurements. In the etching process, the samples were immersed in a 10% KI (by weight) solution for about 2 min. After the KI etching, the samples were immediately rinsed with deionized water for $\sim 2-3$ min. This KI etching treatment removes a surface layer of about 60 μm thickness (i.e., a ~ 30 μm/min etching rate).[12] The fresh ruby red HgI_2 surfaces were blown in dry air to remove the excess water. VASE measurements were performed immediately on the new fresh surfaces.

B. VASE and polarized transmission measurements

The spectroscopic ellipsometry (SE) is designed to accurately determine the values of $\tan(\psi)$ and $\cos(\Delta)$, which are the amplitude and projected phase of the complex reflectance ratio,

$$\rho = r_p / r_s = \tan(\psi) e^{i\Delta}, \tag{1}$$

where r_p and r_s are the reflectance coefficients of light polarized parallel to (p) or perpendicular to (s) the plane of incidence. The ψ and Δ are sensitive to changes of the surface conditions, overlayer thicknesses, dielectric functions, and other parameters of the sample.[13,14]

The pseudodielectric function $\langle\varepsilon\rangle$ is obtained from the ellipsometrically measured values of ρ, in a two-phase model (ambient/substrate):

$$\langle\varepsilon\rangle = \langle\varepsilon_1\rangle + i\langle\varepsilon_2\rangle = \varepsilon_a \left[\left(\frac{1-\rho}{1+\rho} \right)^2 \sin^2 \Phi \tan^2 \Phi + \sin^2 \Phi \right], \tag{2}$$

regardless of the possible presence of surface overlayers.[13] The ε_a in Eq. (2) represents the ambient dielectric function (i.e., $\varepsilon_a = 1$ in vacuum). Since the HgI_2 is a tetragonal crystal, it exhibits uniaxial anisotropy and must be described by two dielectric-response functions $\varepsilon_\perp(\omega)$ and $\varepsilon_\parallel(\omega)$, representing optical electric-field vector-oriented perpendicular (ordinary) and parallel (extraordinary) to the c axis of the crystal, respectively.

Ellipsometric measurement of the complex ratio ρ at a single wavelength and angle of incidence provides two quantities (ψ and Δ), which can be used to determine two parameters describing the sample, e.g., dielectric function ($\varepsilon = \varepsilon_1 + i\varepsilon_2$) of an isotropic bulk sample with no overlayer complications. Spectroscopic (multiple wavelengths) ellipsometric measurements greatly increase the number of determined parameters of the sample, especially when measurements were made at more than one angle of incidence. Thus, VASE makes possible the detailed evaluation of crystals with tetragonal structures.

Multiple angle SE measurements of the two HgI_2 samples at the three special optical configurations, mentioned above, were taken in the range 1.24–5.1 eV with an increment of 0.02 eV, at five different angles of incidence ranging from 67.5° to 77.5° with an increment of 2.5°. Polarized transmission measurements in the same spectral range with the same increment were also made from an a-plane HgI_2 sample with the two optical configurations, i.e., $\mathbf{E}\perp\langle c\rangle$ and $\mathbf{E}\parallel\langle c\rangle$, respectively. The VASE and polarized transmission measurements were made using a variable-angle spectroscopic ellipsometer, which was equipped with a beam-chopped, rotating analyzer to increase the stray light rejection and signal-to-noise ratio.

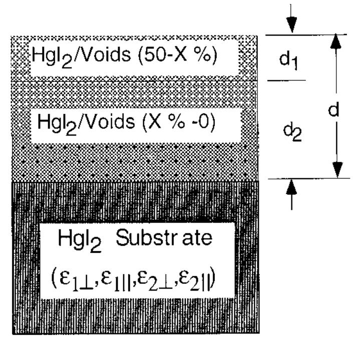

FIG. 1. Surface model for VASE analysis.

A surface model was assumed, for the VASE analysis, including two top graded overlayers, a top surface rough layer, and a subsurface layer representing the distribution of possible surface defects, as shown in Fig. 1. In this model, each surface layer contains more than one constituent. The Bruggeman effective-medium approximation[15] (EMA) is employed to calculate the effective optical constants of the mixed layer. It can be expressed as

$$f_A \frac{\varepsilon_A - \varepsilon}{\varepsilon_A + 2\varepsilon} + f_B \frac{\varepsilon_B - \varepsilon}{\varepsilon_B + 2\varepsilon} = 0, \tag{3}$$

where ε is the effective dielectric function of the mixed layer. The values of ε_A and ε_B are the dielectric functions of the material A and B, respectively, and f_A and f_B are the relative volume fractions. This is based on the assumption of a homogeneous mixture and a random-aggregate spherical microstructure (e.g., a HgI_2 layer with voids). Notice that since HgI_2 is anisotropic, the top two EMA layers, d_1 and d_2, are treated as anisotropic layers, in which $\varepsilon_\perp$ and $\varepsilon_\parallel$ satisfy Eq. (3), respectively. A detailed application of this surface model is presented later in this paper.

VASE data from the three different reflection geometries, from both c-plane and a-plane HgI_2 samples, and the polarized transmission data from the a-plane surface were numerically fitted simultaneously through a multiple-sample and multiple-model regression analysis[16] of the assumed surface model, by varying the anisotropic optical constants of the crystal as well as the surface roughness layer thicknesses and the voids volume percentage until the calculated and measured values match as closely as possible. This is done by minimizing the χ^2 error function defined as

$$\chi^2 = \sum_{i,j} \left\{ \left[\frac{\psi(h\nu_i, \Phi_j) - \psi^C(h\nu_i, \Phi_j)}{\sigma_{i\psi}} \right]^2 + \left[\frac{\Delta(h\nu_i, \Phi_j) - \Delta^C(h\nu_i, \Phi_j)}{\sigma_{i\Delta}} \right]^2 \right\}, \tag{4}$$

where $h\nu$ is the photon energy, Φ is the external angle of incidence, σ is the measured standard deviation of the measurement, and i and j are used to sum over all the photon energies and external angles of incidence, respectively. In all three configurations, the interface reflection Jones matrix r is diagonal.[17]

TABLE I. Fresnel's equations for anisotropic interfaces; the physical meaning of angles of θ_1, θ_{2e}, and α is illustrated in Fig. 2.

Scattering geometry	Polarization	r_{12}	t_{12}
1: c axis normal to boundary (C-P)	p polarization	$r_{12p}=\frac{\sqrt{\varepsilon_{2s}}\cos(\theta_1)-\sqrt{\varepsilon_1}\cos(\alpha)}{\sqrt{\varepsilon_{2s}}\cos(\theta_1)+\sqrt{\varepsilon_1}\cos(\alpha)}$	$t_{12p}=\frac{2\sqrt{\varepsilon_1}\cos(\theta_1)}{\sqrt{\varepsilon_{2s}}\cos(\theta_1)+\sqrt{\varepsilon_1}\cos(\alpha)}$
		$\sqrt{\varepsilon_{2s}}=\frac{\sqrt{\varepsilon_{2\perp}}\sqrt{\varepsilon_{2\parallel}}}{\sqrt{\left[\sqrt{\varepsilon_{2\parallel}}\cos(\theta_{2e})\right]^2+\left[\sqrt{\varepsilon_{2\perp}}\sin(\theta_{2e})\right]^2}}\cos(\theta_{2e}-\alpha)$, $\tan(\alpha)=-\left(\frac{\varepsilon_{2\perp}}{\varepsilon_{2\parallel}}\right)\tan(\theta_{2e})$, $\tan(\theta_{2e})=\frac{\sqrt{\varepsilon_1}\sin(\theta_1)}{\sqrt{\varepsilon_{2\perp}}\left[1-\left(\frac{\varepsilon_1}{\varepsilon_{2\parallel}}\right)(\sin(\theta_1))^2\right]^{1/2}}$.	
	s polarization	$r_{12s}=\frac{\sqrt{\varepsilon_1}\cos(\theta_1)-\sqrt{\varepsilon_{2\perp}}\cos(\theta_{2o})}{\sqrt{\varepsilon_1}\cos(\theta_1)+\sqrt{\varepsilon_{2\perp}}\cos(\theta_{2o})}$	$t_{12s}=\frac{2\sqrt{\varepsilon_1}\cos(\theta_1)}{\sqrt{\varepsilon_1}\cos(\theta_1)+\sqrt{\varepsilon_{2\perp}}\cos(\theta_{2o})}$
		$\sin(\theta_{2o})=\frac{\sqrt{\varepsilon_1}\sin(\theta_1)}{\sqrt{\varepsilon_{2\perp}}}$	
2: c axis in boundary ∥ to plane of incidence (aEp)	p polarization	$r_{12p}=\frac{\sqrt{\varepsilon_{2s}}\cos(\theta_1)-\sqrt{\varepsilon_1}\cos(\alpha)}{\sqrt{\varepsilon_{2s}}\cos(\theta_1)+\sqrt{\varepsilon_1}\cos(\alpha)}$	$t_{12p}=\frac{2\sqrt{\varepsilon_1}\cos(\theta_1)}{\sqrt{\varepsilon_{2s}}\cos(\theta_1)+\sqrt{\varepsilon_1}\cos(\alpha)}$
		$\sqrt{\varepsilon_{2s}}=\frac{\sqrt{\varepsilon_{2\perp}}\sqrt{\varepsilon_{2\parallel}}}{\sqrt{\left[\sqrt{\varepsilon_{2\perp}}\cos(\theta_{2e})\right]^2+\left[\sqrt{\varepsilon_{2\parallel}}\sin(\theta_{2e})\right]^2}}\cos(\theta_{2e}-\alpha)$, $\tan(\alpha)=-\left(\frac{\varepsilon_{2\parallel}}{\varepsilon_{2\perp}}\right)\tan(\theta_{2e})$, $\tan(\theta_{2e})=\frac{\sqrt{\varepsilon_1}\sin(\theta_1)}{\sqrt{\varepsilon_{2\parallel}}\cos(\theta_{2o})}$.	
	s polarization	$r_{12s}=\frac{\sqrt{\varepsilon_1}\cos(\theta_1)-\sqrt{\varepsilon_{2\perp}}\cos(\theta_{2o})}{\sqrt{\varepsilon_1}\cos(\theta_1)+\sqrt{\varepsilon_{2\perp}}\cos(\theta_{2o})}$	$t_{12s}=\frac{2\sqrt{\varepsilon_1}\cos(\theta_1)}{\sqrt{\varepsilon_1}\cos(\theta_1)+\sqrt{\varepsilon_{2\perp}}\cos(\theta_{2o})}$
		$\sin(\theta_{2o})=\frac{\sqrt{\varepsilon_1}\sin(\theta_1)}{\sqrt{\varepsilon_{2\perp}}}$	
3: c axis in boundary ⊥ to plane of incidence (aEs)	p polarization	$r_{12p}=\frac{\sqrt{\varepsilon_{2\perp}}\cos(\theta_1)-\sqrt{\varepsilon_1}\cos(\theta_{2o})}{\sqrt{\varepsilon_{2\perp}}\cos(\theta_1)+\sqrt{\varepsilon_1}\cos(\theta_{2o})}$	$t_{12p}=\frac{2\sqrt{\varepsilon_1}\cos(\theta_1)}{\sqrt{\varepsilon_{2\perp}}\cos(\theta_1)+\sqrt{\varepsilon_1}\cos(\theta_{2o})}$
		$\sin(\theta_{2o})=\frac{\sqrt{\varepsilon_1}\sin(\theta_1)}{\sqrt{\varepsilon_{2\perp}}}$	
	s polarization	$r_{12s}=\frac{\sqrt{\varepsilon_1}\cos(\theta_1)-\sqrt{\varepsilon_{2\parallel}}\cos(\theta_{2e})}{\sqrt{\varepsilon_1}\cos(\theta_1)+\sqrt{\varepsilon_{2\parallel}}\cos(\theta_{2e})}$	$t_{12s}=\frac{2\sqrt{\varepsilon_1}\cos(\theta_1)}{\sqrt{\varepsilon_1}\cos(\theta_1)+\sqrt{\varepsilon_{2\parallel}}\cos(\theta_{2e})}$
		$\sin(\theta_{2e})=\frac{\sqrt{\varepsilon_1}\sin(\theta_1)}{\sqrt{\varepsilon_{2\parallel}}}$	

III. RESULTS

A. Fresnel's equations for anisotropic interfaces

VASE analysis employs the coefficients of reflectance and transmittance as functions of spectral optical dielectric response of each media and the angle of incidence at the boundary of the two media. For isotropic materials, they are well known as Fresnel's equations. For anisotropic media, this issue has been theoretically studied and applied to certain cases.[18] However, the complete analytical expressions including reflection and transmittance are not readily available. In Ref. 17, the study was limited to reflection SE measurements on a bulk anisotropic material. Therefore, only reflection coefficients were derived and used in the ellipsometry analysis. In our studies, reflection VASE and polarized transmission data from anisotropic samples were analyzed

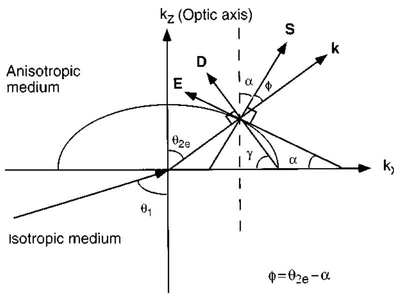

FIG. 2. Refraction by a uniaxial anisotropic medium. The optical axis is in the plane of incidence and perpendicular to the sample surface.

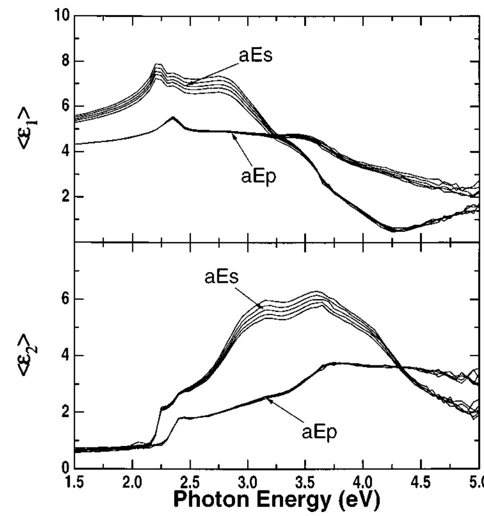

FIG. 3. Pseudodielectric response $\langle\varepsilon\rangle$ of an a-plane single-crystal HgI_2 surface, measured by VASE with *aEp* and *aEs* configuration, respectively, at five different angles of incidence ranging from 67.5° to 77.5° with an increment of 2.5°.

simultaneously in a multiple-model, multiple-sample approach; hence, reflectance and transmittance equations are needed for our VASE analysis. Furthermore, those equations are also needed in studying the anisotropic materials by using transmission VASE measurements.[13] In this section, we present the Fresnel's equations for anisotropic interfaces in the three special optical configurations in Table I.

Those equations were derived based on Maxwell's equations and the properties of uniaxial anisotropic media (crystals). In an isotropic medium, the electric-field **E** and displacement field vector **D** are in the same direction and always normal to the wave propagation and the velocity of a plane wave is a constant independent of the direction of propagation in the medium. Therefore, the refractive indices of an isotropic medium is a sphere corresponding to a constant frequency. These are no longer true in anisotropic media, except for certain particular directions. For uniaxial anisotropic crystals, the electric-field vector **E** and displacement field vector **D** are in general not in the same direction. So does the wave propagation direction represented by the Poynting vector **S** and the direction of the wave vector **k**, as shown in Fig. 2. The angle of incidence θ_1, and other angles θ_{2e} and α, used in the Fresnel's equations listed in Table I are illustrated in Fig. 2.

B. Analysis and discussion

Figure 3 shows pseudodielectric response $\langle\varepsilon\rangle$ of an a-plane single-crystal HgI_2 surface, measured by VASE with aEp and aEs configuration, respectively, at five different angles of incidence ranging from 67.5° to 77.5° with an increment of 2.5°. The obviously different pseudodielectric responses from the aEp and aEs geometries, and angular dispersions of $\langle\varepsilon_1\rangle$ and $\langle\varepsilon_2\rangle$ in both situations provide strong evidence of the uniaxial anisotropic nature of HgI_2 crystal. The c axis of this a-plane sample was at first assumed parallel to one of its cleaved edges. This assumption was proved to be correct in the later VASE analysis.

Polarized transmission measurements were made on the a-plane surface with optical electric-field vector **E** oriented parallel ($\mathbf{E}\|\langle c\rangle$) and perpendicular ($\mathbf{E}\perp\langle c\rangle$) to the c axis, respectively, in a range from 1.24 to 2.5 eV with an increment of 0.02 eV, as shown in Fig. 4.

The HgI_2 surface was modeled as two graded layers containing voids, labeled as d_1 and d_2 in thickness, as shown in Fig. 1. The top layer (d_1) is mainly used to describe the physical roughness of the sample surface, while the sublayer (d_2) is designed to reflect the possible subsurface defects. In the top layer (d_1), the volume voids percentage was linearly graded from 50% to x%, while in the sublayer (d_2) the voids percentage was linearly graded from x% to 0%. The linear grading was achieved by dividing one layer into five thin slices with evenly incremented x values. The effective optical constants of the mixed graded layers used in the VASE analysis were calculated using the Bruggeman EMA. During the VASE regression analysis, the coupled optical constants of the HgI_2 in both bulk and the EMA top layers, $\varepsilon_{1\perp}$, $\varepsilon_{1\|}$, $\varepsilon_{2\perp}$, $\varepsilon_{2\|}$, and the thicknesses of the top (d_1) and subsurface (d_2) layers, plus the voids percentage x in the subsurface layer were varied to fit all the VASE data from two samples in c-p, aEp, and aEs configurations and the polarized transmission data, simultaneously. Each sample was described by its own surface model, the numerical fitting was based on the assumption that the optical constants of the c-plane and a-plane samples are the same and they were

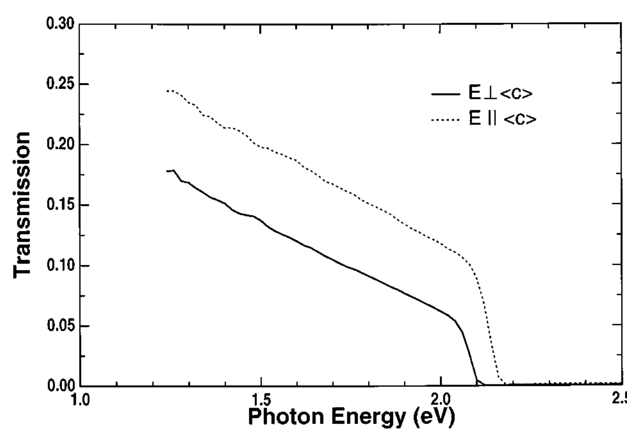

FIG. 4. Polarized transmission of HgI_2.

a-plane sample (N16-12):

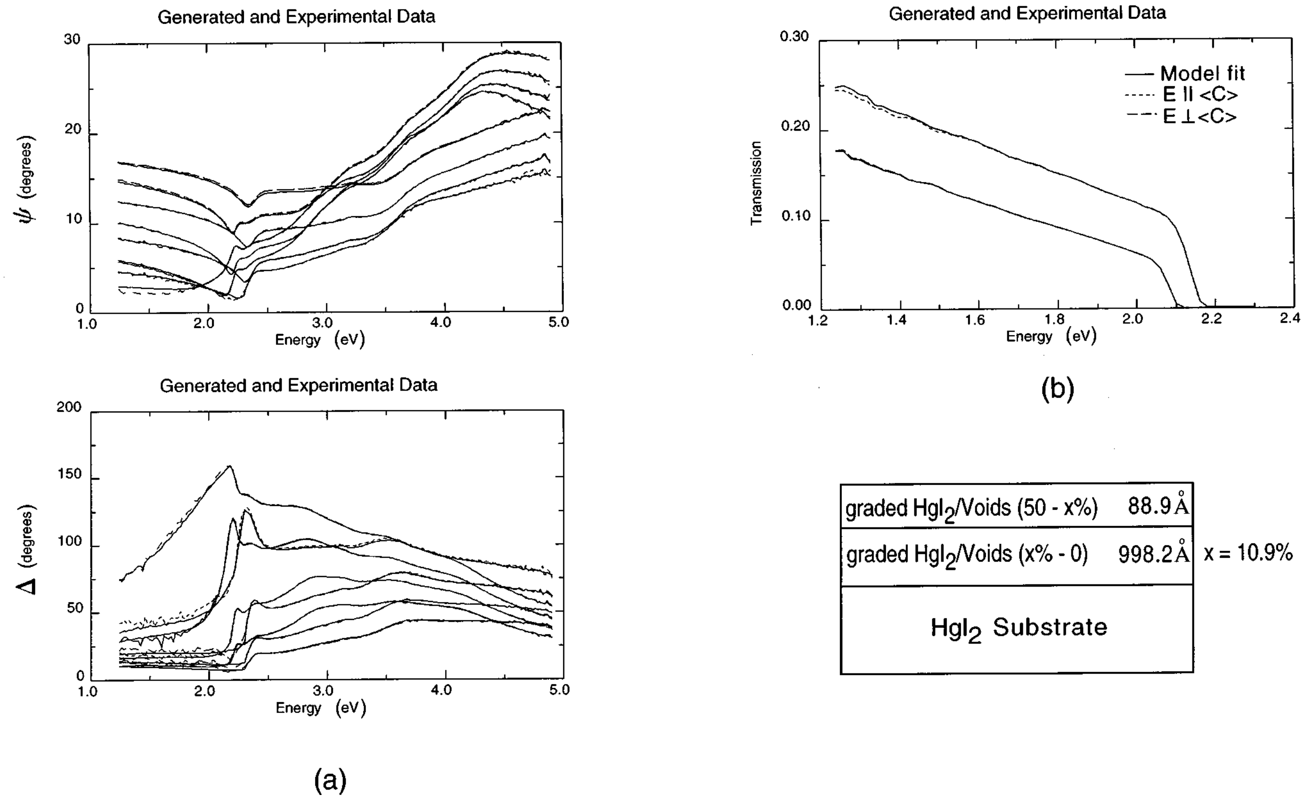

FIG. 5. VASE analysis of the model fit from the *a*-plane HgI_2. The solid line represents the best fit and the dotted or dashed lines are the experimental VASE and transmission data, in (a) and (b), respectively. The sketch at the lower right is the surface model for the analysis.

c-plane sample (N15-21):

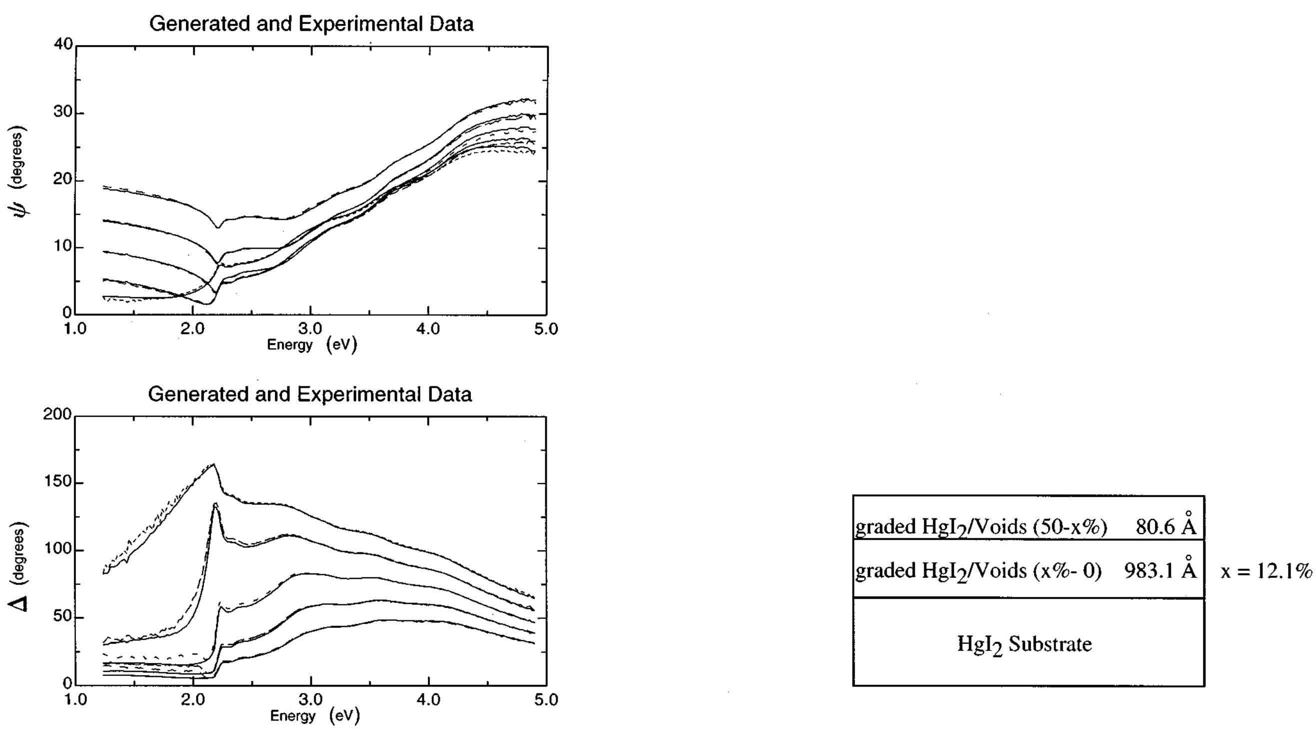

FIG. 6. VASE analysis of the model fit from the *c*-plane HgI_2. This *c*-plane sample was analyzed simultaneously with the *a*-plane sample shown in Fig. 5 via multiple sample VASE analysis.

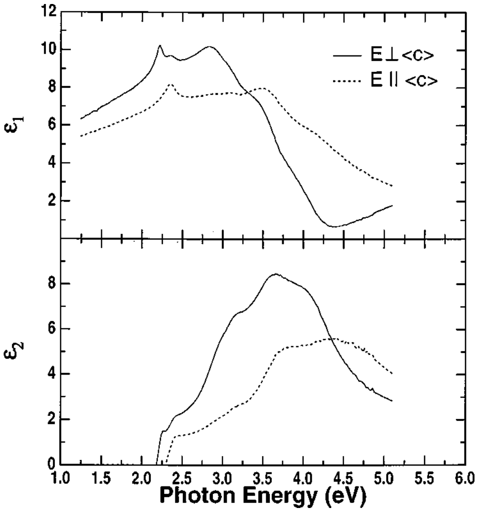

FIG. 7. Anisotropic dielectric functions of HgI_2 with ordinary ($\mathbf{E}\perp c$) and extraordinary ($\mathbf{E}\| c$) responses, respectively.

coupled together through a multiple-sample VASE analysis. The multiple-sample method allows us to analyze several independent VASE data simultaneously, and couple some of the common optical constants together during the numerical fitting. This method greatly increases the ratio of SE determined quantities to fitting parameters, so that reduces the possible coupling between fitting variables.

As an illustration, we show the results of multiple-sample VASE analysis in Figs. 5 (a plane) and 6 (c plane). For the a-plane sample, four angles of incidence of VASE data of each optical configuration (i.e., aEp and aEs, respectively) were fitted, while five angles of incidence VASE data from the c-plane sample were used for analysis. As we can see, the model fit (the solid line) and the experimental data (the dotted or dashed lines) are matched very closely. The VASE analysis shows that this a-plane sample (N16-12) has a top roughness layer of ~88.9 Å followed by a subsurface layer of ~998.2 Å with $x=10.9\%$, while the c-plane HgI_2 sample resulted in thicknesses of 80.6 and 983.1 Å with $x=12.1\%$, for the top and subsurface layer, respectively. We believe the surface roughness layers described by EMA, especially the subsurface layer, are related to surface defects and surface aging of HgI_2 crystal. A detailed study of the surface aging of HgI_2 crystal is reported in a separate paper.[19]

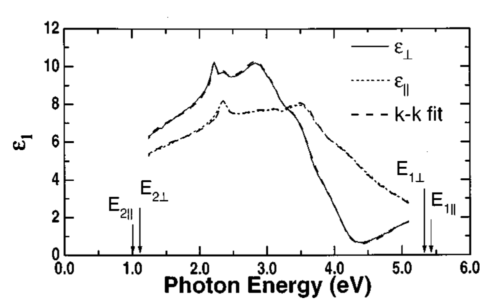

FIG. 8. The Kramers-Kronig fit of the dielectric functions of HgI_2. $\varepsilon_\perp$ and $\varepsilon_\|$ refer to ordinary and extraordinary responses of dielectric functions, respectively.

TABLE II. Parameter values of the KK fit of the dielectric functions of HgI_2.

	$\varepsilon_1^{\text{offset}}$	E_i (eV)	A_i
$E_\perp$	3.516	$E_1=5.3228$, $E_2=1.1079$	$A_1=2.9958$, $A_2=0.3634$
$E_\|$	3.422	$E_1=5.4225$, $E_2=0.9998$	$A_1=5.6906$, $A_2=0.68639$

The surface model with two top graded EMA layers, as shown in Fig. 1, was decided by comparisons of regression analyses on several different surface models, such as bulk only, one top EMA layer with graded or without graded x values, etc. The minimized χ^2 error function, defined in Eq.

TABLE III. Anisotropic optical properties of HgI_2.

eV	$\varepsilon_{1\perp}$	$\varepsilon_{2\perp}$	$\varepsilon_{1\|}$	$\varepsilon_{2\|}$	$\alpha_\perp(10^3\ \text{cm}^{-1})$	$\alpha_\|(10^3\ \text{cm}^{-1})$
5.100	1.792	2.838	2.825	4.050	457.14	531.38
5.000	1.622	3.011	3.009	4.334	480.50	539.56
4.900	1.445	3.191	3.201	4.629	503.79	547.14
4.800	1.190	3.437	3.461	5.052	538.17	561.37
4.700	1.066	3.711	3.642	5.148	563.11	549.77
4.600	0.895	4.143	3.958	5.396	602.88	545.11
4.500	0.772	4.645	4.343	5.495	639.85	526.10
4.400	0.657	5.239	4.685	5.582	678.03	508.66
4.300	0.760	5.968	5.047	5.580	706.60	485.03
4.200	1.144	6.818	5.399	5.501	722.99	457.36
4.100	1.854	7.483	5.705	5.338	711.01	426.61
4.000	2.614	7.839	5.967	5.281	681.38	405.58
3.900	3.317	8.040	6.269	5.257	648.34	386.56
3.800	3.996	8.224	6.711	5.214	617.89	364.13
3.700	4.702	8.400	7.158	5.010	588.43	333.23
3.600	5.867	8.387	7.749	4.442	539.25	280.57
3.500	6.853	7.940	7.953	3.777	478.26	231.45
3.400	7.434	7.327	7.924	3.196	422.35	191.90
3.300	7.808	6.916	7.741	2.795	383.00	165.42
3.200	8.251	6.748	7.647	2.651	355.86	153.22
3.100	8.983	6.369	7.748	2.420	316.46	134.99
3.000	9.538	5.706	7.699	2.167	269.94	117.62
2.900	10.060	4.856	7.683	1.946	219.02	102.36
2.800	10.164	3.841	7.636	1.684	168.08	85.98
2.700	9.907	3.036	7.551	1.506	130.48	74.62
2.600	9.635	2.584	7.508	1.383	108.71	66.21
2.500	9.487	2.300	7.554	1.310	93.93	60.15
2.400	9.595	2.090	7.960	1.200	81.57	51.59
2.300	9.655	1.513	7.892	0.000	56.59	0.00
2.200	10.088	0.395	7.309	0.000	13.87	0.00
2.100	8.902	0.000	6.967	0.000	0.00	0.00
2.000	8.385	0.000	6.719	0.000	0.00	0.00
1.900	8.021	0.000	6.522	0.000	0.00	0.00
1.800	7.729	0.000	6.328	0.000	0.00	0.00
1.700	7.497	0.000	6.152	0.000	0.00	0.00
1.600	7.210	0.000	5.963	0.000	0.00	0.00
1.500	6.987	0.000	5.857	0.000	0.00	0.00
1.400	6.735	0.000	5.695	0.000	0.00	0.00
1.300	6.503	0.000	5.488	0.000	0.00	0.00
1.200	6.259	0.000	5.291	0.000	0.00	0.00

(4), of the proposed surface model was significantly lower than other models. On the other hand, as shown in Fig. 3, the nonzero $\langle \varepsilon_2 \rangle$ values under 2.25 eV (the lower absorption edge observed by the polarized transmission), also suggests a top surface layer structure.

Figure 7 shows the room-temperature (RT) anisotropic dielectric functions of HgI_2 crystal in a range of 1.24–5.1 eV, as results of the VASE analysis. It is noticeable that the absorption edges of the ordinary and extraordinary dielectric response ε_2 are different: $\sim$2.25 eV for the ordinary and $\sim$2.43 eV for the extraordinary response. This is consistent with the results related to the optical transitions between the conduction band and the heavy- and light-hole valence band indicated by theoretical studies.[20]

KK transformation relation was employed to check the consistency of the anisotropic dielectric functions. The KK transformation reflects the nature of relation between the real and imaginary part of the dielectric function $\varepsilon = \varepsilon_1 + i\varepsilon_2$, and can be written as

$$\varepsilon_1(\hbar\omega) = 1 + \frac{2}{\pi} p \int_0^{\infty} \frac{x\varepsilon_2(x)}{x^2 - (\hbar\omega)^2} dx, \tag{5}$$

where $\hbar\omega$ is the photon energy. By the KK transformation, the real part of the dielectric function ε_1 can be obtained through the imaginary part ε_2. However, the KK transformation integrates the entire spectral range, while our VASE measurements are limited in the range of 1.24–5.1 eV. Two nonbroadening oscillators were employed to cover the unmeasured spectral range. The modified KK transformation is written as

$$\varepsilon_1^{\mathrm{KK}}(\hbar\omega) = \varepsilon_1^{\mathrm{offset}} + \sum_{i=1}^{2} \frac{A_i}{(\hbar\omega)^2 - E_i^2} + \frac{2}{\pi} p \int_{1.24\ \mathrm{eV}}^{5.1\ \mathrm{eV}} \frac{x\varepsilon_2^{\mathrm{meas}}(x)}{x^2 - (\hbar\omega)^2} dx, \tag{6}$$

where A_i and E_i are the amplitude and center energy for the ith oscillator, respectively. An $\varepsilon_1^{\mathrm{offset}}$ was used to replace the unit value in the KK relation. Thus, values of $\varepsilon_{2\perp}$ (ordinary) and $\varepsilon_{2\parallel}$ (extraordinary) obtained through VASE analysis were used to calculate $\varepsilon_{1\perp}$ (ordinary) and $\varepsilon_{1\parallel}$ (extraordinary) via the KK relation Eq. (6), respectively. The calculated values were compared with the VASE determined $\varepsilon_{1\perp}$ and $\varepsilon_{1\parallel}$, through a regression analysis by varying the values of A_i, E_i, and $\varepsilon_1^{\mathrm{offset}}$ until calculated and measured values match as closely as possible. The results of the KK fit are shown in Fig. 8 and Table II. It is obvious that a good KK fit was obtained by applying one oscillator on the higher-energy side and one on the lower-energy side for each set of ε, as indicated by the arrows in Fig. 8. The lower-energy-side oscillator is often not needed because of the simple nonabsorbing behavior below the material band gap. However, one oscillator with low-center-energy is needed in this case because of the strong zone-center phonon absorption of HgI_2 crystal.[21]

Selected values of $\varepsilon_\perp(\omega)$ and $\varepsilon_\parallel(\omega)$, shown in Fig. 7, are listed in Table III. Notice that the listed values at 1.2 eV were extrapolated from Fig. 7. Also listed are polarized absorption coefficients of HgI_2, $\alpha_\perp$ and $\alpha_\parallel$, for optical electric-field vector **E** oriented perpendicular and parallel to the c axis, respectively. The absorption coefficients were calculated through $\langle \alpha \rangle = 4\pi \langle k \rangle / \lambda$, where $\langle k \rangle$ is the extinction coefficients of the refractive indices of HgI_2.

IV. CONCLUSIONS

In summary, we have studied the anisotropic optical properties of HgI_2 crystal, by variable angle spectroscopic ellipsometry. Polarized reflectance and transmittance at three special optical-axis configurations, concerning the uniaxial anisotropic nature of the crystal, were derived as functions of angles of incidence to facilitate the VASE analysis. Two surface orientations of the tetragonal crystal were chosen, i.e., an a-plane and a c-plane surface, for the study. Room-temperature anisotropic dielectric functions of HgI_2 crystal, both ordinary $\varepsilon_\perp(\omega)$ and extraordinary $\varepsilon_\parallel(\omega)$, in the range of 1.24–5.1 eV, were extracted by the VASE measurements and multiple-sample and multiple-model analysis. Both dielectric functions satisfy the Kramers-Kronig relation, respectively. Different energy-band absorption edges were observed, at room temperature, from the ordinary and extraordinary dielectric responses at 2.25 and 2.43 eV, respectively. They are related with optical transitions between the conduction band and the heavy- and light-hole valence band.

ACKNOWLEDGMENTS

This work was supported by the Department of Energy via Sandia National Laboratories. A helpful discussion with Dr. G. E. Jellison, for checking the numerical results of the anisotropic Fresnel's equations, is greatly appreciated.

[1] W. R. Wing, Nucl. Instrum. Methods **96**, 615 (1971).

[2] S. P. Swierkowski, G. A. Armantrout, and R. Wichne, IEEE Trans. Nucl. Sci. **NS-21**, 302 (1974).

[3] J. P. Ponpon, R. Stuck, P. Siffert, B. Meyer, and C. Schwab, IEEE Trans. Nucl. Sci. **22**, 182 (1975).

[4] A. J. Dabrowski, W. M. Szymczyk, J. S. Iwanczyk, J. H. Kusmiss, W. Drummond, and L. Ames, Nucl. Instrum. Methods **213**, 89 (1983).

[5] J. H. Howes and J. Watling, in *Nuclear Radiation Detector Materials*, edited by E. E. Heller, H. W. Kraner, and W. A. Higinbótham MRS Symposia Proceedings No. 16 (Materials Research Society, Pittsburgh, 1983), p. 207.

[6] B. V. Novikov and M. M. Pimonenko, Sov. Phys. Semicond. **4**, 1785 (1971).

[7] K. Kanzaki and I. Imai, J. Phys. Soc. Jpn. **32**, 1003 (1972).

[8] A. Aneda, F. Raga, E. Grilli, and M. Guzzi, Nuovo Cimento B **38**, 439 (1977).

[9] P. D. Bloch, J. W. Hodby, C. Schwab, and D. W. Stacey, J. Phys. C. **11**, 2579 (1978).

[10] A. Anedda, E. Grilli, M. Guzzi, F. Raga, and A. Serpi, Solid State Commun. **39**, 1121 (1981).
[11] T. Goto and A. Kasuya, J. Phys. Soc. Jpn. **50**, 520 (1981).
[12] X. J. Bao, T. E. Schlesinger, R. B. James, R. H. Stulen, C. Ortale, and A. Y. Cheng, J. Appl. Phys. **68**, 86 (1990).
[13] R. M. A. Azzam and N. M. Bashara, *Ellipsometry and Polarized Light* (North-Holland, Amsterdam, 1977).
[14] H. Yao, P. G. Snyder, and J. A. Woollam, J. Appl. Phys. **70**, 3261 (1991).
[15] D. E. Aspnes, J. B. Theeten, and F. Hottier, Phys. Rev. B **20**, 3292 (1979).
[16] This analysis was performed by using the WVASE software from J. A. Woollam Co.
[17] A. Yariv and P. Yen, *Optical Waves in Crystals* (Wiley, New York, 1984).
[18] W. H. Weber, J. T. Remillard, J. R. McBride, and D. E. Aspnes, Phys. Rev. B **46**, 15 085 (1992).
[19] H. Yao, L. A. Lim, R. B. James, M. Schieber, and M. Natarajan, Nucl. Instrum. Methods **380**, 26 (1996).
[20] Y. C. Chang and R. B. James, Phys. Rev. B **46**, 15 040 (1992).
[21] H. K. Sim and Y. C. Chang, Phys. Rev. B **49**, 4559 (1994).